Chemical Physics Letters 664 (2016) 77–82

Contents lists available at ScienceDirect

Chemical Physics Letters

journal homepage: www.elsevier.com/locate/cplett

Research paper

Temperature effects in static and dynamic polarizabilities from distinct generalized gradient approximation exchange-correlation functionals

Javier Carmona-Espíndola [a], José L. Gázquez [a,*], Alberto Vela [b], S.B. Trickey [c]

[a] Departamento de Química, Universidad Autónoma Metropolitana-Iztapalapa, Av. San Rafael Atlixco 186, México, D.F. 09340, Mexico
[b] Departamento de Química, Centro de Investigación y de Estudios Avanzados, Av. Instituto Politécnico Nacional 2508, México, D.F. 07360, Mexico
[c] Quantum Theory Project, Dept. of Physics and Dept. of Chemistry, P.O. Box 118435, University of Florida, Gainesville, FL 32611-8435, USA

ARTICLE INFO

Article history:
Received 30 June 2016
In final form 5 October 2016
Available online 6 October 2016

Keywords:
Density functional theory
Exchange-correlation functional
Exchange potential asymptotic behavior
Polarizabilities
Hyperpolarizabilities
Molecular dynamics

ABSTRACT

To demonstrate that there are specific temperature effects in the description of static and dynamic polarizabilities which arise from generalized gradient approximation exchange-correlation functionals that obey distinctive asymptotic constraints, we present calculations for a test set of small molecules, at the experimental geometry, at the optimized ground-state geometry, and at the Born-Oppenheimer molecular dynamics geometries that arise from simulating a temperature of 300 K. The results indicate that a functional with the correct asymptotic potential (CAP) provides a better description at room temperature than does a GGA functional with an exponentially decaying exchange potential such as PBE.

1. Introduction

The development of exchange-correlation (XC) energy functionals in the Kohn-Sham formulation of density functional theory belonging to different rungs of Jacobs' ladder is a very active area of research [1]. In particular, the generalized gradient approximation (GGA) rung has received great attention, because it is computationally less demanding than higher rung approximations, and at the same time, it is an important component of those. The X GGA energy functional can be expressed in terms of an analytical expression of the X enhancement factor $F_X(s)$ as [2]

$$E_X^{LDA}[\rho] = \int \rho(\mathbf{r})(e_X^{LDA}[\rho](\mathbf{r}))\,F_X(s)\,d\mathbf{r}, \tag{1}$$

where $e_X^{LDA}[\rho](\mathbf{r}) = -(3/4)(3/\pi)^{1/3}(\rho(\mathbf{r}))^{1/3}$ is the local density approximation for the exchange energy per particle, $\rho(\mathbf{r})$ is the electron number density, and $s(\mathbf{r}) = |\nabla\rho(\mathbf{r})|/2(3\pi^2)^{1/3}(\rho(\mathbf{r}))^{4/3}$, is the exchange reduced density gradient. Non-empirical construction based on constraint satisfaction yields an analytical expression for $F_X(s)$. Almost all the available constraints apply to the small- and large-s limits, so $F_X(s)$ is the result of interpolating between those limits. However, neither of those limits is associated with a unique constraint. When $s \to 0$, one has $F_X(s) \to 1 + \mu s^2 + \ldots$, where the constant μ may be fixed through several non-empirical procedures [3–5]. When $s \to \infty$ there are different limiting behaviors, depending on the constraint imposed [2,4,6–9].

Detailed numerical study has established that the description of thermodynamic, kinetic, and structural properties depends primarily on the behavior of the GGA X functional in the reduced density gradient interval $0 \leqslant s \leqslant 3$. On the other hand, the description of excitation energies and response properties such as static and dynamic polarizabilities and hyperpolarizabilities has a strong dependence on the behavior of the exchange potential in the asymptotic region, which for a GGA corresponds to the case when $s \to \infty$. In this context, we proposed the CAP (correct asymptotic potential) X energy functional [8]. On the interval $0 \leqslant s \leqslant 3$ it has a similar enhancement factor to that of PBE and other GGAs, but behaves as [10] $F_X(s) \to (4\pi/3)s$ when $s \to \infty$, so that the functional derivative leads to an X potential that behaves as $-1/r$ when $r \to \infty$. Most other GGAs, including the highly popular PBE [4], have an X potential that decays faster than $-1/r$ when $r \to \infty$, in most cases exponentially. The CAP X energy functional combined with PBE correlation, CAP-PBE, gives heats of formation, ionization potentials, electron affinities, proton affinities, binding energies of weakly interacting systems, barrier heights for hydrogen and non-hydrogen transfer reactions, bond distances, and harmonic frequencies on standard test sets that are competitive with results from other GGAs. However, for the static and dynamic

* Corresponding author.
E-mail addresses: jcarmona_26@yahoo.com.mx (J. Carmona-Espíndola), jlgm@xanum.uam.mx (J.L. Gázquez).

http://dx.doi.org/10.1016/j.cplett.2016.10.014
0009-2614/

polarizabilities and hyperpolarizabilities it was observed that the values obtained with CAP-PBE were, in general, lower than the experimental ones, while the values obtained with LDA and other GGAs, were, in general, equal to or larger than the experimental ones. Since the calculated values were determined without taking into account thermal effects and the experimental values were obtained at room temperature [11–17], we argued that because the theoretical values would be increased by incorporation of temperature effects, CAP-PBE would lead to a better description of these properties.

Thus, the objective of the present work is to quantify the temperature effects in the calculation of static and dynamic polarizabilities and hyperpolarizabilities with time-dependent density functional theory [18,19].

2. Computational methodology

Temperature effects are very important in the description of static and dynamic polarizabilities and hyperpolarizabilities. These effects may be quantified through several procedures [20–22]. In particular, Born-Oppenheimer molecular dynamics (BOMD) simulations have been applied successfully to the description of dipole static polarizabilities [21] and to dipole-quadrupole dynamic polarizabilities [22] of clusters. Thus, in the present work we have considered a test set of twenty two molecules at 300 K, since the majority of the experimental results reported in the literature are for room temperature. In our test set, only water and benzene are in the liquid phase at that temperature. The other systems are in the gas phase.

A rather critical aspect of the calculations concerns the XC energy functional used to drive the BOMD and then the static and dynamic polarizabilities. However, regarding the choice of XC energy functionals considered here, it is relevant that in our previous work we performed calculations with diverse GGAs such as PBE [4], BLYP [7,23], OLYP [23,24] and PBE-LS [6], in addition to LDA. The X components of these GGAs have different $s \to \infty$ behaviors. The enhancement factor of PBE tends to a constant value of 1.804 that comes from enforcing the local Lieb-Oxford bound. The BLYP enhancement factor diverges as $(s/\ln s)$ to reproduce the asymptotic behavior of the conventional (canonical) exact exchange energy density, while in OLYP the enhancement factor approaches a constant value of 2.59 (from parametrizing the OPTX analytical expression through minimizing the X-only error with respect to Hartree-Fock total energies for the neutral atoms from H to Ar). The PBE-LS enhancement factor decays to zero to fulfill the non-uniform density scaling result [25]. Despite these gross differences in enhancement factor asymptotic behaviors, all of those functionals tended to overestimate the values of static and dynamic polarizabilities and hyperpolarizabilities studied in that work. Thus, in the present work we consider temperature effects only for PBE and CAP-PBE, because it can be expected that the tendencies observed for PBE will be similar for the other GGAs.

The X enhancement factor of PBE is [4]

$$F_X^{PBE}(s) = 1 + \kappa - \frac{\kappa}{1 + \frac{\mu s^2}{\kappa}}, \tag{2}$$

where $\kappa = 0.804$ and $\mu = 0.2195$. These parameter values were determined non-empirically from constraint satisfaction. For CAP, the enhancement factor is [8]

$$F_X^{CAP}(s) = 1 + \mu \frac{s \ln(1+s)}{1 + (3\mu/4\pi)\ln(1+s)} \tag{3}$$

where $\mu = 0.2195$ (as in PBE) also was set non-empirically by constraint satisfaction.

All calculations reported here were performed with the code deMon2k [26], pre-release version 4.2.9. Geometry optimizations and BOMD simulations were done with the DZVP/GEN-A2 combination of orbital and auxiliary density basis sets. The MD trajectory for each molecule [21,22,27] was calculated at 300 K for the PBE and CAP-PBE functionals. Each trajectory had a length of 80 ps with a time step of 2 fs. The temperature in the canonical BOMD simulation was controlled by a Nose-Hoover chain thermostat. To determine the temperature dependence of the polarizabilities, the polarizability tensor was calculated along the recorded trajectories. To this end, the first 20 ps of each trajectory were discarded. The static and dynamic polarizabilities, $\bar{\alpha}(\omega)$, were calculated for the remaining 60 ps with a 100 fs interval between polarizability calculations. All static and dynamic polarizabilities were obtained via time-dependent auxiliary density perturbation theory (TDADPT) [28–32]. The orbital and auxiliary basis sets for the calculation of the temperature-dependent part of the polarizabilities were TZVP-FIP1 [33]/GEN-A2* [34] respectively. The reason for this selection is based on the fact that it has been shown that basis sets for polarizabilities calculations must contain diffuse functions [35]. A strategy for constructing such basis sets is to augment valence basis sets of good quality with additional polarization functions [36–38]. The TZVP-FIP1 basis set used here [33] is built

Table 1
Comparison of PBE and CAP static polarizabilities [au] of small molecules with respect to experimental values.

Molecule	Experimental geometry		Optimized geometry		BOMD geometries (300 K)		Exp.
	PBE	CAP	PBE	CAP	PBE	CAP	
HF	5.94	5.55	6.04	5.66	6.05	5.67	5.40[a]
C_2H_2	23.32	21.96	23.94	22.59	24.08	22.76	22.80[b]
CH_3F	17.54	16.71	18.16	17.35	18.32	17.51	17.32[b]
H_2S	24.41	23.15	24.94	23.70	25.01	23.78	24.66[c]
CH_2F_2	18.45	17.57	19.17	18.35	19.32	18.50	18.20[b]
OCS	34.03	32.38	34.61	32.92	34.73	32.99	34.44[b]
SO_2	25.72	24.47	27.02	25.68	27.09	25.76	25.49[d]
CHF_3	19.67	18.70	20.24	19.35	20.39	19.49	18.69[b]
CF_4	20.02	19.11	20.86	20.02	21.00	20.15	19.53[e]
MAD	0.43	0.81	0.94	0.50	1.05	0.53	
MD	0.28	−0.77	0.94	−0.10	1.05	0.01	

[a] Static value from refractive index dispersion [12].
[b] Static value from refractive index dispersion [15].
[c] Extrapolated static value from dispersion of dynamic mean polarizability [15].
[d] Static value from refractive index and Rayleigh scattering dispersion [15].
[e] Static value from refractive index dispersion [11].

Table 2
Comparison of PBE and CAP dynamic polarizabilities [au] of small molecules with respect to experimental values.

Molecule	Experimental geometry		Optimized geometry		BOMD geometries (300 K)		Exp.
	PBE	CAP	PBE	CAP	PBE	CAP	
N_2	11.94	11.45	12.19	11.69	12.21	11.67	11.76[a]
CO	13.66	12.97	13.89	13.20	13.89	13.20	13.34[b]
HCl	17.74	16.85	17.94	17.05	17.96	17.09	17.54[b]
O_2	10.67	10.16	10.95	10.41	10.98	10.48	10.57[a]
N_2O	19.83	19.07	20.41	19.51	20.46	19.60	20.24[b]
CO_2	17.80	16.97	18.31	17.45	18.34	17.49	17.53[a]
Cl_2	30.75	29.36	31.54	30.12	31.61	30.21	31.11[b]
C_2H_4	28.79	27.24	29.27	27.79	29.50	28.02	28.48[b]
C_2H_6	30.07	28.49	30.95	29.46	31.29	29.81	30.16[b]
MAD	0.24	0.91	0.52	0.45	0.61	0.35	
MD	0.06	−0.91	0.52	−0.45	0.61	−0.35	

[a] Values derived from precise interferometric measurements of the refractive index at λ = 632.8 nm and 300 K [17].
[b] Depolarized light scattering at λ = 632.8 nm [13].

from the triple zeta valence plus polarization (TZVP) basis set optimized for local DFT calculations [39]. On the other hand, it is important to mention that some static polarizability calculations performed with the aug-cc-pVTZ [40] indicate that the basis set employed in this work yields practically the same results as those obtained with those very large basis sets. For consistency with our previous work [14] as well as with the literature generally, we evaluated the TDDFT kernel in the adiabatic local density approximation (ALDA) [41–44]. That is, the LDA second functional derivatives were used rather than the PBE or CAP derivatives. As in our previous work [8], the exchange-correlation energy, potential and kernel were integrated numerically with the so-called reference grid [45] in deMon2k. The mean static and dynamic polarizabilities were calculated from the diagonal elements of the frequency dependent polarizability tensor,

$$\bar{\alpha}(\omega) = \frac{1}{3}(\alpha_{xx}(\omega) + \alpha_{yy}(\omega) + \alpha_{zz}(\omega)) \quad (4)$$

The calculations reported in the next section were done at the experimental geometry, at the optimized ground state geometry, and at the Born-Oppenheimer molecular dynamic geometries that arise from simulating a temperature of 300 K. In the latter case the value of the property corresponds to the average of the values obtained at each geometry.

3. Results and discussion

Table 1 presents static polarizabilities of nine small molecules, together with the mean absolute deviation (MAD) and mean deviation (MD) with respect to the experimental values at room temperature. One can see that for the set of single point calculations at the experimental geometries [46–48], PBE gives a better description than CAP with MADs of 0.43 and 0.81 au, respectively. However, when the calculations are done at the optimized geometries for each of the two functionals, one finds that CAP performs better than PBE, with a MAD of 0.50 versus 0.94 au. When the geometries of the BOMD trajectories are used, one finds that CAP provides an even better description than PBE, with MADS of 0.53 (CAP) and 1.05 au (PBE).

Table 2 shows the results for the dynamic polarizabilities of nine other small molecules. All dynamic polarizabilities were determined at the wavelength of 632.8 nm, which corresponds to the experimental value. As in the case of the static polarizabilities, on the single-point calculations at the experimental geometries [47–49] PBE, with a MAD of 0.24 performs better than CAP with a MAD of 0.91. Once again, the relationship changes upon going to the optimized geometries for the two functionals. Then the MAD for PBE is 0.52 au, while for CAP it is 0.45. Finally, when one considers the 300 K BOMD trajectories, the advantage of CAP is even larger, with a MAD for PBE of 0.61 versus 0.35 for CAP geometries.

Table 3
Comparison of PBE and CAP optimized geometries of the molecules considered in the present work with respect to experimental values (distances in angstroms and angles in degrees).

Molecule		PBE	CAP	EXP
HF	R(H-F)	0.936	0.938	0.917
C_2H_2	R(C-C)	1.221	1.223	1.203
	R(C-H)	1.078	1.080	1.063
CH_3F	R(C-H)	1.110	1.112	1.087
	R(C-F)	1.403	1.408	1.383
	∡ (CFH)	108.86	108.26	108.73
	∡ (HCH)	110.70	110.67	110.20
H_2S	R(H-S)	1.337	1.368	1.338
	∡ (HSH)	94.62	95.37	91.60
CH_2F_2	R(C-F)	1.378	1.383	1.351
	R(C-H)	1.113	1.115	1.084
	∡ (FCF)	108.67	108.38	108.49
	∡ (HCH)	113.42	114.09	112.80
	∡ (HCF)	108.67	108.54	108.87
OCS	R(C-O)	1.182	1.182	1.160
	R(C-S)	1.579	1.577	1.560
SO_2	R(S-O)	1.483	1.482	1.430
	∡ (OSO)	119.03	119.28	119.30
CHF_3	R(C-H)	1.112	1.115	1.098
	R(C-F)	1.360	1.363	1.332
	∡ (FCF)	108.50	108.60	108.83
	∡ (FCH)	110.42	110.34	110.10
CF_4	R(C-F)	1.346	1.349	1.315
N_2	R(N-N)	1.120	1.119	1.098
CO	R(C-O)	1.152	1.153	1.128
HCl	R(H-Cl)	1.301	1.303	1.275
O_2	R(O-O)	1.239	1.236	1.208
N_2O	R(N-N)	1.154	1.153	1.128
	R(N-O)	1.208	1.205	1.184
CO_2	R(C-O)	1.183	1.183	1.162
Cl_2	R(Cl-Cl)	2.043	2.042	1.988
C_2H_4	R(C-C)	1.340	1.342	1.339
	R(C-H)	1.101	1.103	1.086
	∡ (HCH)	117.36	117.51	117.60
	∡ (CCH)	121.32	121.24	121.20
C_2H_6	R(C-C)	1.533	1.535	1.536
	R(C-H)	1.109	1.112	1.091
	∡ (HCH)	107.88	107.99	107.99
	∡ (CCH)	111.02	110.91	110.91
H_2O	R(O-H)	0.976	0.977	0.958
	∡ (HOH)	104.47	104.71	104.51
NH_3	R(N-H)	1.027	1.029	1.012
	∡ (HNH)	106.80	107.06	106.67
CH_4	R(C-H)	1.106	1.109	1.087
Benzene	R(C-C)	1.401	1.405	1.404
	R(C-H)	1.100	1.102	1.102

In Table 3 we present a comparison between the optimized geometries obtained with the PBE and CAP functionals, and the experimental values. One can see that both functionals lead to very similar results that reproduce reasonably well the experimental geometries. Thus, it could be inferred from these results that the differences in the polarizabilities values with CAP and PBE come basically from the differences in the orbitals and eigenvalues obtained with an exponentially and a $-1/r$ decaying potentials. See Tables 8 and 9 and Figs. 6 and 7 of Ref. [8].

Figs. 1–4 show dynamic mean polarizabilities of H_2O, NH_3, CH_4, and benzene, respectively. Again single-point polarizabilities were calculated at experimental structures [47,49,50]. In the case of water (Fig. 1) one can see that PBE leads to larger values than the experimental ones [14,16]. The results that are closer to the experimental ones correspond to the single-point calculations done with the experimental geometries, while the results with the optimized geometry and those with the BOMD trajectory geometries overestimate even more the dynamic polarizabilities. For CAP the single-point calculations done with the experimental geometries give values below the experimental ones. However, the results with the optimized geometry and those with the BOMD trajectory lead to rather good agreement with experiment. A relevant aspect is related to the fact that, as shown in Fig. 1, the dynamic polarizability results at the experimental geometry determined with a high level *ab initio* method like time dependent MC-SCF [16], lead to results that lie very close to those obtained

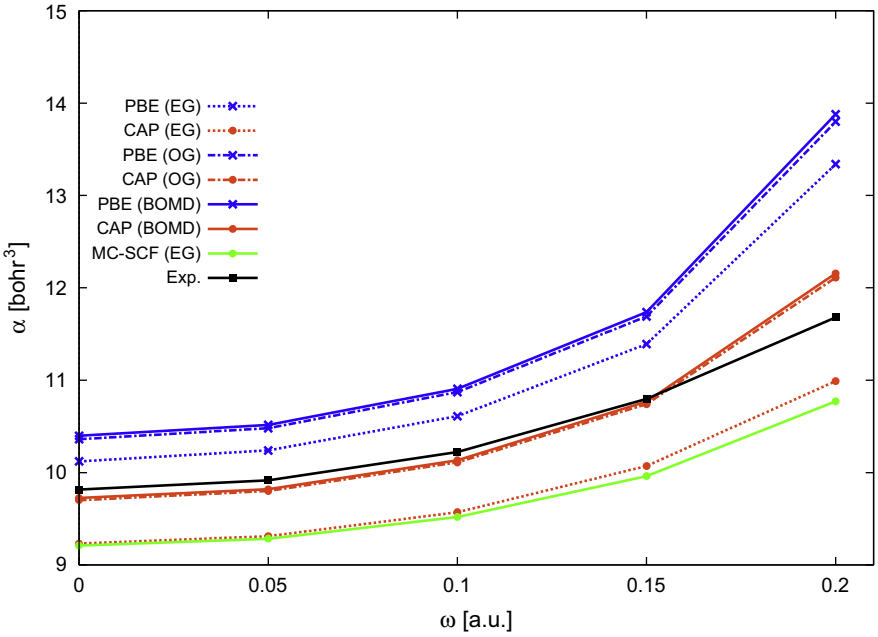

Fig. 1. Comparison of the static and dynamic polarizabilities of H_2O as a function of ω determined from the experimental geometry (EG), the optimized geometry (OG) and the BOMD geometries at 300 K.

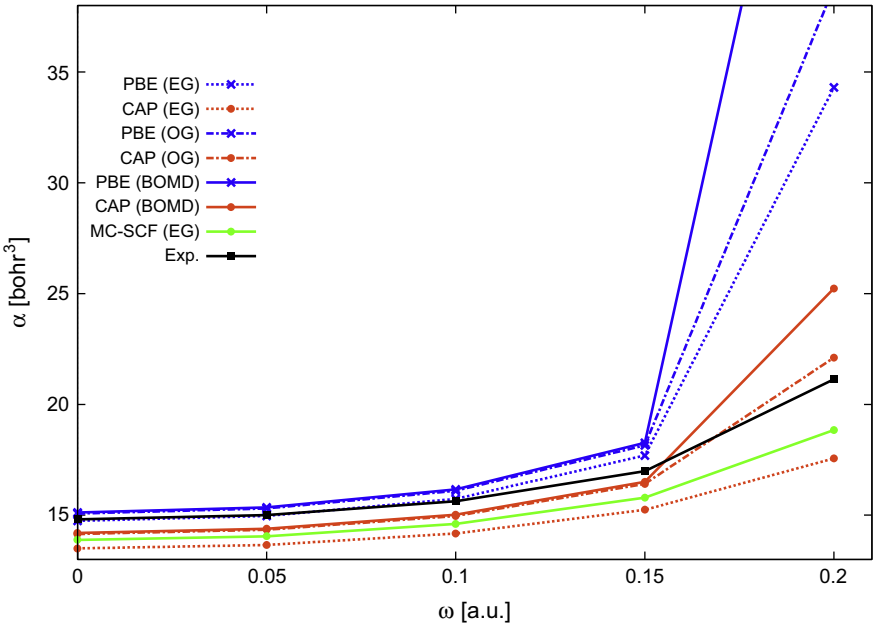

Fig. 2. As in Fig. 1 for NH_3.

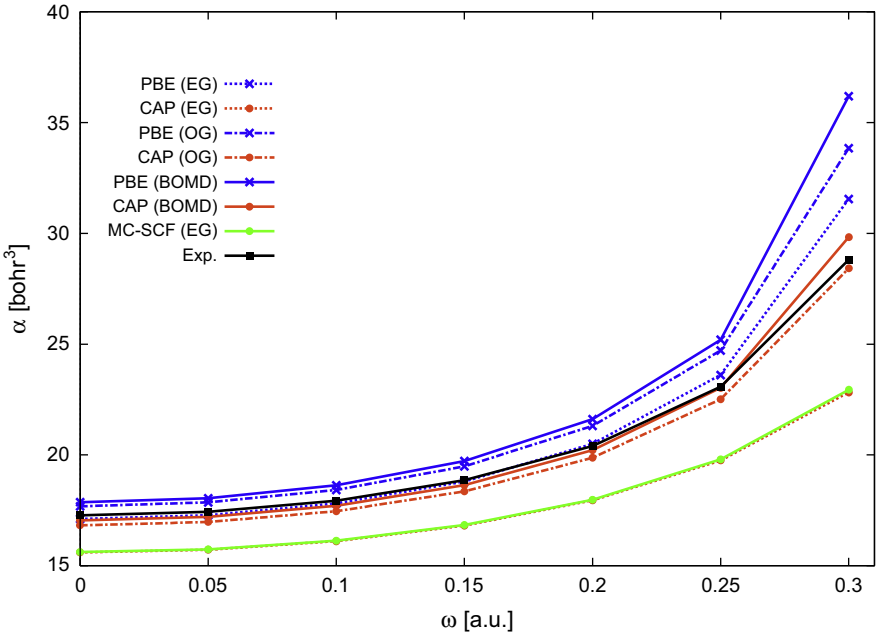

Fig. 3. As in Fig. 1 for CH_4.

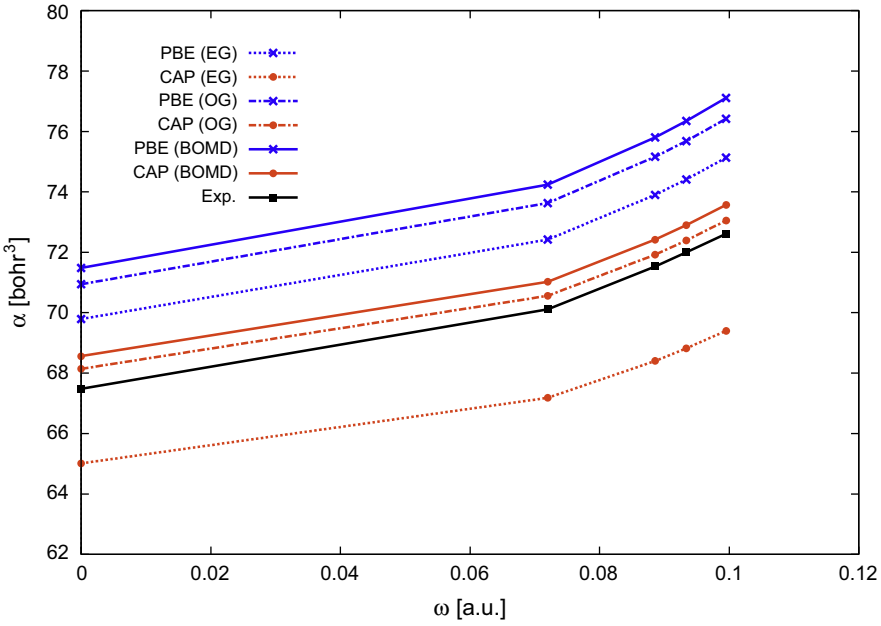

Fig. 4. As in Fig. 1 for Benzene.

with CAP, indicating that indeed, the latter provides a better description of this property at a temperature of 0 K than PBE, and that, as expected, thermal effects increase the values. That is, PBE at 0 K overestimates the polarizability, so that it fortuitously lies closer to the experimental geometry, but when thermal effects are included, the PBE values increase and show a larger deviation from the experimental ones. The results for ammonia and methane follow a very similar pattern, although in those cases the PBE single-point calculations at the experimental geometries lead to values that lie rather close to the experimental ones. But when the optimized geometry or the BOMD trajectory geometries are used, PBE leads to a larger overestimation, while CAP gets closer to the experimental values. Again, the dynamic polarizability results obtained with CAP at the experimental geometry are in very good agreement with time dependent MC-SCF values [16]. It is worth to mentioning that in the case of ammonia the pole polarizability for PBE seems to occur at lower frequencies than CAP and experimental polarizabilities, causing a much larger deviation. Finally, one can see in Fig. 4 that the pattern for benzene is very similar to the one obtained for water in Fig. 1, although in this case the results with optimized geometry are slightly better than the ones corresponding to the BOMD geometries.

4. Conclusions

The results presented in this work indicate that the description provided by PBE worsens as one moves from the single-point

calculations at the experimental geometry to calculations with the optimized geometry and with geometries from BOMD trajectories. In contrast, the description provided by CAP improves along that sequence of geometries. Thus, one may reason that correct asymptotic behavior of the exchange potential is an important factor for an adequate description of response properties, like the static and dynamic polarizabilities and, on the other hand, that thermal effects are also very important for a satisfactory description of these properties.

As was mentioned before, the results shown for PBE are very similar to the ones obtained with other GGA functionals that lead to potentials that decay faster than $-1/r$, as may be seen in Ref. [8].

It is important to mention a matter of context for that argument. The CAP potential has an uncommon behavior, as can be seen in the plots presented in Ref. [8]. That feature leads to a localization of the lowest unoccupied molecular orbital (LUMO) which is higher than usual, and which seems to be at least partly responsible for the improved description of response properties. The correct asymptotic behavior of CAP occurs at large distances from the molecule. Thus there is opportunity for functional development that would modify the enhancement factor given by Eq. (3), in order to yield the $-1/r$ behavior at shorter distances than in CAP and without a peculiarly shaped potential at intermediate r.

Acknowledgments

We thank the Laboratorio de Supercómputo y Visualización of Universidad Autónoma Metropolitana-Iztapalapa for the use of their facilities. JCE was supported in part by CONACYT and by Universidad Autónoma Metropolitana through postdoctoral fellowships. JLG thanks Conacyt for grant 237045, and AV thanks Conacyt for grant 128369. SBT was supported in part by U.S. NSF grant DMR-1515307.

References

[1] A.D. Becke, J. Chem. Phys. 140 (2014) 18A301.
[2] J.P. Perdew, W. Yue, Phys. Rev. B 33 (1986) 8800.
[3] P.R. Antoniewicz, L. Kleinman, Phys. Rev. B 31 (1985) 6779.
[4] J.P. Perdew, K. Burke, M. Ernzerhof, Phys. Rev. Lett. 77 (1996) (erratum 78, 1396 (1997) 3865).
[5] L.A. Constantin, E. Fabiano, S. Laricchia, F. Della Sala, Phys. Rev. Lett. 106 (2011) 186406.
[6] J.L. Gázquez, J.M. del Campo, S.B. Trickey, R.J. Alvarez-Mendez, A. Vela, in: S.K. Ghosh, P.K. Chattaraj (Eds.), Concepts and Methods in Modern Theoretical Chemistry, CRC Press, Boca Raton, 2013, p. 295.
[7] A.D. Becke, Phys. Rev. A 38 (1988) 3098.
[8] J. Carmona-Espindola, J.L. Gázquez, A. Vela, S.B. Trickey, J. Chem. Phys. 142 (2015) 054105.
[9] S.H.L. Li, D.G. Truhlar, J. Chem. Theor. Comput. 11 (2015) 3123.
[10] E. Engel, J.A. Chevary, L.D. Macdonald, S.H. Vosko, Z. Phys. D: At., Mol. Clusters 23 (1992) 7.
[11] H.E. Watson, K.L. Ramaswamy, Proc. R. Soc. Lond., Ser. A 156 (1936) 144.
[12] A.J. Perkings, J. Phys. Chem. 68 (1964) 654.
[13] N.J. Bridge, A.D. Buckingham, Proc. R. Soc. Lond., Ser. A 295 (1966) 334.
[14] G.R. Alms, A.K. Burnham, W.H. Flygare, J. Chem. Phys. 63 (1975) 3321.
[15] M.P. Bogaard, A.D. Buckingham, R.K. Pierens, A.H. White, J. Chem. Soc., Faraday Trans. 1 74 (1978) 3008.
[16] E.A. Reinsch, J. Chem. Phys. 83 (1985) 5784.
[17] K. Kerl, U. Hohm, H. Varchmin, Ber. Bunsenges. Phys. Chem. 96 (1992) 728.
[18] M. Petersilka, U.J. Gossmann, E.K.U. Gross, Phys. Rev. Lett. 76 (1996) 1212.
[19] M.E. Casida, in: J.M. Seminario (Ed.), Recent Developments and Applications in Density Functional Theory, Elsevier, Amsterdam, 1996, p. 391.
[20] K. Ruud, P.O. Astrand, P.R. Taylor, J. Chem. Phys. 112 (2000) 2668.
[21] G.U. Gamboa, P. Calaminici, G. Geudtner, A.M. Köster, J. Phys. Chem. A 112 (2008) 11969.
[22] S.V. Shedge, S. Pal, A.M. Köster, Chem. Phys. Lett. 552 (2012) 146.
[23] C.T. Lee, W.T. Yang, R.G. Parr, Phys. Rev. B 37 (1988) 785.
[24] N.C. Handy, A.J. Cohen, Mol. Phys. 99 (2001) 403.
[25] M. Levy, J.P. Perdew, Phys. Rev. B 48 (1993) (erratum 55, 13321 (1997) 11638).
[26] G. Geudtner, P. Calaminici, J. Carmona-Espíndola, J.M. del Campo, V.D. Domínguez-Soria, R. Flores-Moreno, G.U. Gamboa, A. Goursot, A.M. Köster, J. U. Reveles, T. Mineva, J.M. Vásquez-Pérez, A. Vela, B.Z. Gutiérrez, D.R. Salahub, Wiley Interdiscipl. Rev.: Comput. Mol. Sci. 2 (2012) 548.
[27] A. Goursot, T. Mineva, J.M. Vásquez-Pérez, P. Calaminici, A.M. Köster, D.R. Salahub, Phys. Chem. Chem. Phys. 15 (2013) 860.
[28] R. Flores-Moreno, A.M. Köster, J. Chem. Phys. 128 (2008) 134105.
[29] S.V. Shedge, J. Carmona-Espíndola, S. Pal, A.M. Köster, J. Phys. Chem. A 114 (2010) 2357.
[30] J. Carmona-Espíndola, R. Flores-Moreno, A.M. Köster, J. Chem. Phys. 133 (2010) 084102.
[31] J. Carmona-Espíndola, R. Flores-Moreno, A.M. Köster, Int. J. Quantum Chem. 112 (2012) 3461.
[32] P. Calaminici, J. Carmona-Espíndola, G. Geudtner, A.M. Köster, Int. J. Quantum Chem. 112 (2012) 3252.
[33] P. Calaminici, K. Jug, A.M. Köster, J. Chem. Phys. 109 (1998) 7756.
[34] P. Calaminici, F. Janetzko, A.M. Köster, R. Mejía-Olvera, B. Zúniga-Gutiérrez, J. Chem. Phys. 126 (2007) 044108.
[35] H.J. Werner, W. Meyer, Mol. Phys. 31 (1976) 855.
[36] A.J. Sadlej, Collect. Czech. Chem. Commun. 53 (1988) 1995.
[37] G.D. Zeiss, W.R. Scott, N. Suzuki, D.P. Chong, S.R. Langhoff, Mol. Phys. 37 (1979) 1543.
[38] M. Jaszunski, B.O. Roos, Mol. Phys. 52 (1984) 1209.
[39] N. Godbout, D.R. Salahub, J. Andzelm, E. Wimmer, Can. J. Chem. 70 (1992) 560.
[40] A.S. Karne, N. Vaval, S. Pal, J.M. Vasquez-Perez, A.M. Koster, P. Calaminici, Chem. Phys. Lett. 635 (2015) 168.
[41] M. Gruning, O.V. Gritsenko, S.J.A. Van Gisbergen, E.J. Baerends, J. Chem. Phys. 114 (2001) 652.
[42] S.J.A. van Gisbergen, J.G. Snijders, E.J. Baerends, J. Chem. Phys. 109 (1998) 10657.
[43] M. Stener, G. Fronzoni, M. De Simone, Chem. Phys. Lett. 373 (2003) 115.
[44] M. Seth, G. Mazur, T. Ziegler, Theor. Chem. Acc. (2011) 331.
[45] A.M. Köster, R. Flores-Moreno, J.U. Reveles, K.P. Huber, J. Chem. Phys. 121 (2004) 681.
[46] R.L. Cook, F.C. DeLucia, P. Helminger, J. Mol. Struct. 28 (1975) 237.
[47] G. Herzberg, Electronic Spectra and Electronic Structure of Polyatomic Molecules, Van Nostrand Reinhold Company, New York, 1966.
[48] K.P. Huber, G. Herzberg, Molecular Spectra and Molecular Structure IV. Constants of Diatomic Molecules, Van Nostrand, New York, 1979.
[49] E. Hirota, J. Mol. Spectrosc. 77 (1979) 213.
[50] A.R. Hoy, P.R. Bunker, J. Mol. Spectrosc. 74 (1979) 1.